## POLITECNICO DI TORINO
## Repository ISTITUZIONALE

Effects of exhaust gas recirculation in diesel engines featuring late PCCI type combustion strategies

*Terms of use:*

(Article begins on next page)

07 August 2024

# EFFECTS OF EXHAUST GAS RECIRCULATION IN DIESEL ENGINES FEATURING LATE PCCI TYPE COMBUSTION STRATEGIES

*d'Ambrosio, S*[*], and Ferrari, A.

*Energy Department – Politecnico di Torino*

*C.so duca degli Abruzzi, 24, 10129, Torino, Italy.*

## 1. ABSTRACT

The influence of exhaust gas recirculation (*EGR*) has been analyzed considering experimental results obtained from a Euro 5 diesel engine calibrated with an optimized pilot-main double injection strategy. The engine features a late premixed charge compression ignition (*PCCI*) type combustion mode and different steady-state key-points that are representative of the engine application in a passenger car over the New European Driving Cycle (*NEDC*) have been studied. The engine was fully instrumented to obtain a complete overview of the most important variables. The pressure time history in the combustion chamber has been measured to perform calculations with single and three-zone combustion diagnostic models. These models allow the in-cylinder emissions and the temperature of the burned and unburned zones to be evaluated as functions of the crankshaft angle.

The *EGR* mass fraction was experimentally varied within the 0÷50% range. The results of the investigation have shown the influence that high *EGR* rates can have on intake and exhaust temperatures, in-cylinder pressure and heat release rate time histories, engine-out emissions (*CO*, *HC*, *NO$_x$*, soot), brake specific fuel consumption and combustion noise for a *PCCI* type combustion strategy. The outputs of the diagnostic models have been used to conduct a detailed analysis of the cause-and-effect relationships between the *EGR* rate variations and the engine performance. Finally, the effect of the *EGR* on the cycle-to-cycle variability of the engine torque has been experimentally investigated.

**Highlights:**

- The effects that a high *EGR* rate can have on *PCCI* type combustion strategies have been analyzed.

- The dependence of engine emission and combustion noise on *EGR* has been addressed.

---

[*] Corresponding author e-mail address: stefano.dambrosio@polito.it

25     -    The time histories of the main in-cylinder variables have been plotted for different *EGR* rates.

## 2.   INTRODUCTION.

27    Conventional diesel engines are lean burning systems, if the overall air-fuel ratios are considered [1]. A premixed

28    combustion phase is followed by a mixing-controlled combustion stage, in which the oxidation reactions are much

29    faster than the diffusion rate of the fuel in the charge [2, 3]. Most of the fuel burns in the diffusion controlled phase and

30    the flames are located at approximately stoichiometric regions within the overall lean, but locally inhomogeneous

31    mixture. As a consequence, high flame temperatures, which can be estimated through adiabatic stoichiometric

32    temperature calculations [4, 5], are obtained in the presence of oxygen and nitrogen and large amounts of $NO_x$ are

33    therefore generated [6, 7]. Diffusive combustion is also responsible for most of the soot generation [2] because of the

34    presence of rich pockets within the cylinder, which cannot find the necessary oxygen amount during the later stages of

35    combustion, especially when the engine is working at high loads [1].

36    External exhaust gas recirculation (*EGR*) is a strategy that is adopted in diesel engines to reduce combustion flame

37    temperatures, which are responsible for high $NO_x$ formation. The result of *EGR* utilization is that most of the elemental

38    nitrogen is emitted as harmless $N_2$ [8-13]. Furthermore, *EGR* also has a positive effect on engine noise because it limits

39    the heat release rate (*HRR*) during premixed combustion, which is usually characterized by rapid burning fuel [14].

40    However, the application of the *EGR* can determine penalties in terms of engine emissions and performance, such as

41    particulate matter (*PM*), *CO*, unburned hydrocarbons (*HC*) and a deterioration in the brake specific fuel consumption

42    (*bsfc*) [15-18]. In particular, extremely high values of *EGR* negatively affect the diffusive combustion process, as they

43    increase the soot emissions and induce a rise in the cycle-to-cycle variability of combustion [1]. Nevertheless, the

44    increase in soot generation for increasing *EGR* rates determines higher radiation and a consequent decrease in the flame

45    temperatures that can help to further diminish $NO_x$ emissions [8]. Finally, *EGR* can adversely affect the quality of the

46    lubricating oil and engine durability because of increased wear between the piston rings and the cylinder liner [11, 19-

47    21].

48    The benefits, with respect to the $NO_x$ emissions, depend on the various effects induced by *EGR*: a dilution effect, a

49    thermal effect and a chemical effect [8, 13, 22, 23]. The dilution effect of *EGR* involves a decrease in the in-cylinder

50    oxygen concentration of the inducted charge with the main consequence of decelerating the mixing process between the

51    injected fuel and oxygen. In addition, the quantity of inert gas that can absorb the heat release increases, and this gives

52    rise to lower flame temperatures.

53    The thermal effect consists of an increase in the heat capacity of the inducted charge, because of the augmented average

54    specific heat of the exhaust gas, which contains large amounts of $CO_2$ and $H_2O$, i.e. triatomic gases, compared to fresh

55　air, which mainly contains $O_2$ and $N_2$, i.e. diatomic gases. The $CO_2$ and $H_2O$ concentrations in the exhaust gas are low at

56　part loads, due to an overall leaner mixture, and, as a result, $EGR$ is more effective at high loads [4, 11]. As a

57　consequence, high $EGR$ levels are required to drastically reduce the $NO_x$ emissions at low loads [9]. Another effect,

58　which should be included in the thermal effect of $EGR$, is due to the increase in the inlet temperature of the charge as

59　the $EGR$ rate is augmented, since the exhaust gas temperature is higher than that of fresh air. Therefore, a reduction in

60　the charge density and in the in-cylinder trapped mass is obtained as the $EGR$ rate grows under constant boost pressure.

61　This behavior is referred to as thermal throttling [2, 8] and it determines a negative effect on $NO_x$ reduction, since it

62　tends to increase the maximum temperature of the burned gas, because of the higher temperature of the induced charge

63　and roughly the same energy of the fuel absorbed by a smaller in-cylinder mass. The negative effect of thermal

64　throttling can prevail over the beneficial thermal effect of the increased specific heat [24] in the final determination of

65　the maximum burned gas temperature. Therefore, the utilization of cooled $EGR$ is recommended [6, 25] in order to

66　mitigate the negative effect of thermal throttling (if the cooled $EGR$ temperature were the same as that of the fresh air,

67　thermal throttling would not be present) and thus to limit the maximum in-cylinder temperature of the burned gas. The

68　benefits of the cooled $EGR$ strategy augment at high $EGR$ rates, and advantages can also be observed in terms of $bsfc$

69　and soot control [12].

70　The third main effect of $EGR$ is of chemical nature and is due to the $CO_2$ and $H_2O$ species that are present in the exhaust

71　gas and which tend to dissociate during combustion, thus reducing the peak combustion temperature and contributing to

72　the inhibition of $NO_x$ formation.

73　When the $EGR$ strategy is applied to a diesel engine, the three previously mentioned effects are present simultaneously.

74　If a part of the oxygen content is replaced by $EGR$ in the cylinder, the given amount of injected fuel has to diffuse over

75　a wider volume before a sufficient stoichiometric mixture can be formed. The thus obtained larger stoichiometric region

76　contains additional quantities of $CO_2$, $H_2O$ and $N_2$, which can absorb part of the combustion-released energy and

77　undergo dissociation phenomena, which lead to even lower flame temperatures [10, 22].

78　Several experiments have been performed with the purpose of evaluating the individual impact of the three

79　abovementioned effects [8, 22]. The dilution effect is responsible for most of the $NO_x$ reduction, and the second effect,

80　in terms of potential, is the chemical one, while the thermal effect is generally the least important [24, 2].

81　As far as the influence of $EGR$ on the fuel ignition delay is concerned [26, 27], the drop in the oxygen concentration,

82　due to the dilution effect, slows down the auto-ignition reactions and enlarges the ignition delay, whereas the thermal

83　throttling effect exerts an opposite influence [8], due to the abovementioned temperature increase of the induced charge.

84　The dilution effect generally prevails over thermal throttling and the ignition delay therefore usually increases with the

85  *EGR* rate and allows more fuel to be evaporated and mixed with the air before combustion starts: the final result is an

86  intensified premixed combustion mode [26].

87  New engine concepts related to low-temperature combustion (*LTC*), such as homogeneous charge compression ignition

88  (*HCCI*) and partial premixed charge compression ignition (*PCCI*), are based on the utilization of large amounts of *EGR*

89  in order to obtain a remarkable reduction in both $NO_x$ and *PM* engine out emissions without aftertreatment systems [28],

90  which require space, additional costs and complexities [29]. High *EGR* rates reduce peak burned gas temperatures and

91  prolong the ignition delay, thus promoting the dispersion of the injected fuel in the charge in order to obtain highly

92  premixed combustion. The engine *bsfc* also improves in the *LTC*, due to almost instantaneous combustion. Although

93  *LTC* is a highly promising strategy, it is still difficult to control the combustion and to extend the strategy to the medium

94  and high–load range of the engine [30, 31]. Furthermore, the *HC* and *CO* emissions at low engine loads represent a

95  major concern for the low temperature combustion typology [32, 33]. In fact, the quantity of supplied fuel at light loads

96  is small and oxidation reactions are quite slow, due to the very lean mixture and low temperatures [34]. The ignition

97  delay is extended and this leads to increased over-mixed areas that are outside the fuel flammability limits [33].

98  Furthermore, retarded main injection timings, which are typical of late *PCCI* combustion strategies, further decrease

99  peak in-cylinder temperatures. Over-mixing and bulk quenching mechanisms are considered the dominant causes of the

100  increased *HC* and *CO* emissions in *PCCI* engines. In addition, impingement can also occur in engines managed with

101  early *PCCI* combustion modes.

102  The practical implementation of the *EGR* strategy is straightforward for naturally aspirated diesel engines, because the

103  backpressure in the exhaust tailpipe is normally higher than the intake pressure [1]. A long-route (or low-pressure) *EGR*

104  loop [35] can be applied to turbocharged diesel engines, since a positive differential pressure is generally available

105  between the turbine outlet and the compressor inlet. However, conventional compressors and intercoolers are not

106  designed to endure diesel exhaust gas temperatures and high fouling levels. Therefore, the preferred solution would be

107  to recycle the exhaust gas from upstream of the turbine to downstream of the compressor in the intake manifold, i.e. a

108  short-route (or high-pressure) *EGR* loop would be adopted. However, this *EGR* layout is only applicable when the

109  upstream pressure of the turbine is sufficiently higher than the boost pressure [1]. An efficient exploitation of the

110  exhaust gas can be obtained by adopting a variable geometry turbine that can effectively provide the desired pressure

111  level upstream of the turbine [23, 25]. In these systems, the *EGR* control is closely related to the variable geometry

112  turbine control [36]. A very high *EGR* rate leads to an appreciable decrease in the gas flow through the turbine, and

113  hence to a possible consequent decrease in boost pressure. For this reason, it is not feasible that a considerable reduction

114  in $NO_x$ could be achieved without any penalties on soot emissions for most short-route *EGR* layouts. Possible

115 improvements could be obtained by applying twin-stage turbocharger setups or by combining high-pressure and low-

116 pressure *EGR* layouts [8].

117 The present work explores the influence of cooled *EGR* mass fractions for values of up to around 50% for a Euro 5 low

118 compression ratio diesel engine, equipped with a twin-stage turbocharger and run on a late *PCCI* type combustion

119 strategy. Even though the *EGR* strategy has been studied extensively in conventional diesel engines with up to 30-40%

120 *EGR* rates [35, 37], a great deal of attention is still being paid to the effects of multiple injections in the presence of

121 heavy *EGR* rates [38, 39], which are typical of *LTC* applications. *EGR* trade-offs have been performed under different

122 steady-state working conditions that correspond to the installation of the engine on a *D*-segment vehicle that runs the

123 European emission homologation cycle. The investigation was based on experimental results obtained at the test bench.

124 Furthermore, simulations were performed using one- and three-zone combustion diagnostic models to investigate the

125 cause-and-effect relationships of the physical events.

## 3.  EXPERIMENTAL SET-UP.

127 The experimental tests have been carried out on the highly-dynamic test bed installed at the Politecnico di Torino

128 ICEAL (IC Engines Advanced Laboratory). The test bench was equipped with an 'ELIN AVL APA 100' cradle-

129 mounted AC dynamometer, while an 'AVL KMA 4000' with a reading accuracy of 0.1% over a 0.28-110 kg/h range

130 was used to continuously meter the fuel consumption. Furthermore, an 'AVL AMAi60' system, made up of three

131 analyzer trains, was utilized to measure the raw engine-out gaseous emissions. Two analyzer trains were equipped with

132 devices for the analysis of the *HC*, $CH_4$, $NO_x$, *CO*, $CO_2$ and $O_2$ species. The third analyzer train included a detector,

133 which was used to measure the $CO_2$ levels in the intake manifold, in order to evaluate the *EGR* rate. Finally, an AVL

134 415S smokemeter allowed the soot emissions in the exhaust gases to be evaluated.

135 The test engine was fully instrumented with piezoresistive pressure transducers and thermocouples in order to measure

136 the pressure and temperature in the intake, exhaust and *EGR* lines of the engine. A high-frequency piezoelectric

137 transducer was installed in the glow-plug seat to measure the pressure time-history of the gases in the combustion

138 chamber of one cylinder and one of the piezoresistive transducers was used to detect the pressure level in the inlet

139 runner of the same cylinder and thus to reference the in-cylinder pressure. All of the abovementioned measurement

140 devices are controlled by the PUMA OPEN 1.3.2 and the Indicom 1.6 automation systems.

141 The engine, whose main features are reported in Table 1, features a low compression ratio (16.3:1), which is in line with

142 typical *PCCI* applications. The twin-stage turbocharger is controlled by means of two waste-gate valves. The short-

143 route *EGR* system includes a cooled *EGR* valve on the exhaust side, which is controlled on the basis of the airflow

144 feedback signal; a shell and tube type *EGR* cooler is placed before this valve. Furthermore, a throttle valve assembly has

145 been placed in the intake system, downstream of the engine intercooler and just upstream of the junction with the *EGR*

146 gases. The use of intake throttling increases the pressure drop in the *EGR* loop, and thus allows the *EGR* rate to be

147 increased at low loads.

| Engine type | 2.0L Euro 5 |
|---|---|
| Displacement | 1956 cm$^3$ |
| Bore x stroke | 83.0 mm x 90.4 mm |
| Compression ratio | 16.3 |
| Valves per cylinder | 4 |
| Turbocharger | Twin-stage with valve actuators and waste-gate |
| Fuel injection system | Common Rail 2000 bar piezo |
| Specific power and torque | 71 kW/l – 205 Nm/l |

**Table 1: Main specifications of the reference engine.**

| Key-point | $SOI_{Pil}$ (°bTDC) | $q_{Pil}$ (mm$^3$/cyl) | $SOI_{Main}$ (° bTDC) |
|---|---|---|---|
| 1500×2 | 11 | 1.7 | –2 |
| 1500×5 | 12 | 1.6 | –1 |
| 2000×2 | 16 | 1.5 | –1 |
| 2000×5 | 17 | 1.4 | 0 |
| 2500×8 | 25 | 1.2 | 4 |
| 2750×12 | 31 | 1.1 | 7 |

**Table 2**: **ECU parameters for the different key-points.**

148 The engine was preliminarily calibrated by applying an optimized pilot-main double injection strategy, which in the

149 present work is referred to as the baseline calibration. Steady-state tests were performed at some engine key-points,

150 which were considered representative of the engine application to a *D*-segment passenger car over the new European

151 driving cycle (*NEDC* ). The considered key-points were expressed in terms of *n* (rpm) × *bmep* (bar) as follows: 1500×2,

152 1500×5, 2000×2, 2000×5, 2500×8, 2750×12.

153 Table 2 reports the values of the pilot injection fuel quantity per cycle and per cylinder ($q_{Pil}$) as well as the injection

154 timing for both the pilot ($SOI_{Pil}$) and main ($SOI_{Main}$) injection pulses. Negative values of $SOI_{Main}$ mean that the injection

155 occurred after the *TDC*. The quantity of the main injection was set automatically by the test bench control system in

156 order to maintain the desired *bmep* value. As can be inferred, the main injection timing is delayed at low loads and the

157 pilot-to-main injection dwell times are long, in line with late *PCCI* strategies.

158 *EGR* trade-off curves were carried out at each key-point in the neighborhood of the baseline calibration point by

159 varying the quantity of inducted air-per-cylinder and stroke, while keeping all the other engine parameters fixed.

160 The *EGR* mass fraction is defined as the ratio of the recirculated exhaust gas mass flow-rate to the total mass flow-rate

161 that is inducted in the cylinder [9, 12]:

$$X_{EGR} = \frac{\dot{m}_{EGR}}{\dot{m}_{EGR} + \dot{m}_a} \qquad (1)$$

where $\dot{m}_{EGR}$ and $\dot{m}_a$ are the *EGR* and fresh-air mass flow-rates, respectively. In the present investigation the calculation of $X_{EGR}$ was performed considering the accurate expression developed in [40], which requires the evaluation of the volume concentrations of all the species at the engine exhaust and knowledge of the combustion air composition at the engine inlet. The *EGR* mass fraction can also be estimated by $CO_2$ volume concentration measurements in the intake manifold $[CO_2]_{int}$, and at the engine exhaust $[CO_2]_{exh}$ according to the following simplified formula, where $[CO_2]_{amb}$ represents the $CO_2$ volume concentration in the external environment:

$$X_{EGR} = \frac{[CO_2]_{int} - [CO_2]_{amb}}{[CO_2]_{exh} - [CO_2]_{amb}} \qquad (2)$$

## 4. STEADY-STATE TESTS.

The *EGR* trade-off curves are plotted for the different key-points with distinct symbols, which are reported in the legend of each graph. The baseline calibration points are highlighted in each diagram with a thin line that contours the corresponding symbol.

The global air-fuel ratio, λ, is reported in Fig. 1 as a function of $X_{EGR}$ for the different key-points. It can be observed that, for the baseline calibration key-points, the lower the load, the higher the adopted *EGR* rate: $X_{EGR} \approx 45 \div 50\%$ at the lowest load (*bmep* = 2 bar), $X_{EGR} \approx 30 \div 35\%$ at medium load (*bmep* = 5 bar) and $X_{EGR} \approx 20 \div 25\%$ at the highest loads (*bmep* = 8 and *bmep* = 12 bar). These values are higher than those usually applied in conventional diesel engines [35, 37].

The application of *EGR* limits the volume available for fresh air within the cylinder. The λ variable is generally shown to decrease almost linearly with $X_{EGR}$ for any key-point, because the quantity of fuel is almost independent of the *EGR* mass fraction at fixed load [12]. A deviation of the λ-$X_{EGR}$ curve from linearity can be noticed for the highest values of
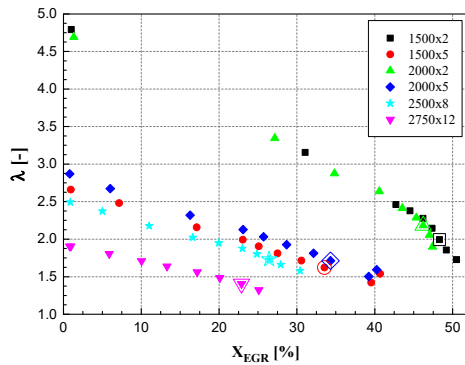


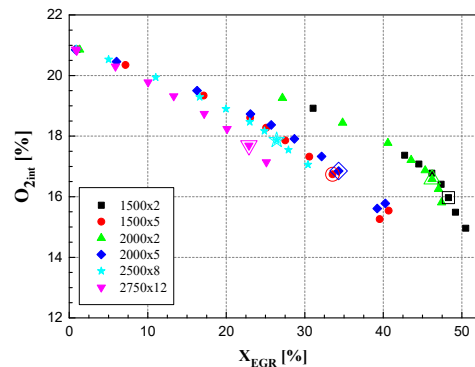Figure 1. Relative air-fuel ratio λ versus $X_{EGR}$



Figure 2. Oxygen volume concentration versus $X_{EGR}$.

181    $X_{EGR}$. In these conditions, a high mass flow-rate of gases is sent back from the engine exhaust to the intake manifold,

182    bypassing the turbine, whereas the fresh-air flow is decreased using the intake throttle valve. As a consequence, it is not

183    possible to maintain the desired level of boost pressure ($p_{int}$), which is set by the *ECU*, in the intake manifold for

184    $X_{EGR} \geq 40\%$, due to both the insufficient enthalpy flux of the exhaust gases entering the turbine and to air throttling,

185    which reduces the pressure level in the manifold. Therefore, both the air mass flow-rate and λ decrease more than

186    proportionally with the *EGR* mass fraction for $X_{EGR} \geq 40\%$.

187    Figure 2 shows that an increase in $X_{EGR}$ has a great impact on the dilution effect, because it can reduce the oxygen

188    volume concentration $[O_2]_{int}$ in the intake manifold to a great extent, compared to the value of around 21%, which

189    corresponds to the oxygen concentration in environmental air. In particular, *EGR* is more effective at high loads than at

190    low loads, because the same $[O_2]_{int}$ can be obtained with a smaller $X_{EGR}$. In fact, as already mentioned, the $CO_2$ and $H_2O$

191    concentrations in the exhaust gas are lower at lighter loads, since the concentrations of these species increase with the

192    equivalence ratio $\phi = 1/\lambda$. Therefore, relatively high *EGR* rates are required at low loads in order to obtain significant

193    reductions in $NO_x$ emissions. This explains why, the lower the load for the baseline calibration key-points in Fig. 1, the

194    higher the $X_{EGR}$. In general, the load dependence of the $[O_2]_{int}$ reduction on $X_{EGR}$ is significant, whereas the influence of

195    the engine speed on the $[O_2]_{int}$-$X_{EGR}$ curves is negligible.

196    The inlet temperature of the in-cylinder charge also rises with the *EGR* rate (Fig. 3). This produces a thermal throttling

197    effect that occurs because the *EGR* cooler is not able to cool the recirculated exhaust gas to the same temperature as the

198    air downstream of the intercooler. The higher the load or the speed, the higher the temperature of the gases at the engine

199    exhaust and the higher the $T_{int}$ temperature for a given $X_{EGR}$ value. Thermal throttling is also induced by the increased

200    internal residual gas fraction (internal *EGR*) that results from the growth of the exhaust manifold pressure as $X_{EGR}$

201    increases. In particular, the pressure difference between the exhaust manifold and the intake manifold, which is

202    responsible for the internal *EGR*, grows significantly for $X_{EGR} \geq 40\%$, because of the intake throttle valve action.
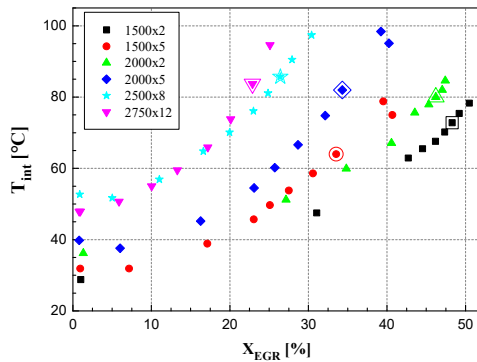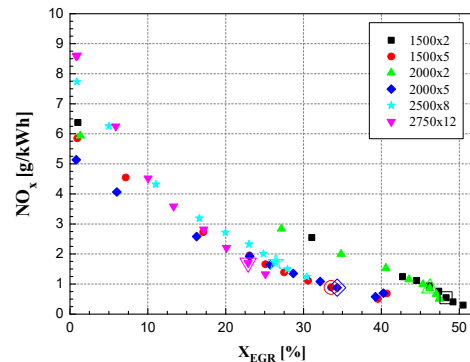


**Figure 3. Engine inlet temperature versus $X_{EGR}$.**
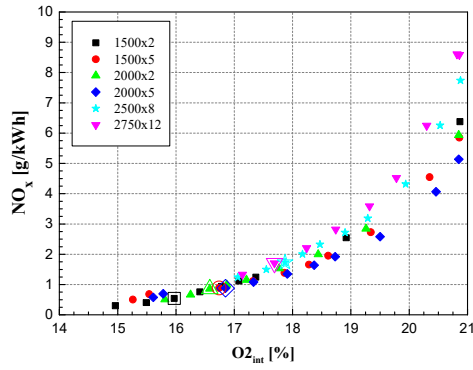
**Figure 4. $NO_x$ emissions versus $X_{EGR}$.**

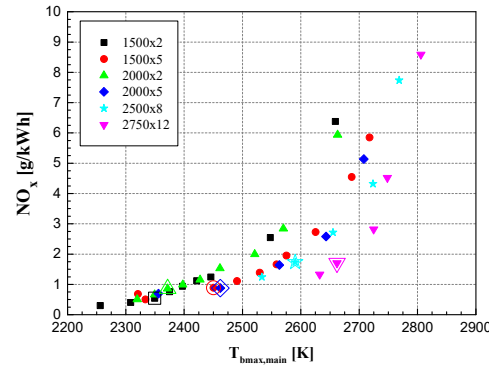Figure 5. *NO$_x$ emissions versus O$_2$.*



Figure 6. *NO$_x$ emissions versus T$_{bmax,main}$.*

203   Figures 4 and 5 show the dependence of the specific $NO_x$ emissions on the *EGR* rate and on the corresponding oxygen

204   volume concentration in the intake manifold, respectively. Dilution is the effect that has most influence on the

205   remarkable reduction in $NO_x$, as the $X_{EGR}$ increase determines the $[O_2]_{int}$ diminution that can be observed in Fig. 5.

206   Results, which are in agreement with those in Fig. 4, were obtained for conventional combustion mode diesel engines in

207   [12, 18, 26] and in [27], where a reduction of approximately 50% was achieved in the $NO_x$ emissions under $X_{EGR} \approx 20\%$

208   for medium load and speed. A better defined trend, which is almost independent of the specific key-point, can be seen

209   more easily in Fig. 5 than in Fig. 4.

210   The reduction in the $NO_x$ species at *bmep*=2 bar and *bmep*=5 bar is also due to the retarded main injection timing

211   (cf. $SOI_{Main}$ in Table 2), which postpones the combustion well into the expansion stroke. In *PCCI* type engines, retarded

212   injection can be a complementary strategy to *EGR* for $NO_x$ control, even though the former leads to increased fuel

213   consumption and deteriorates *HC* emissions [11, 27].

214   In general, $NO_x$ emissions are mainly affected by two factors: the presence of oxygen in the charge and the peak value

215   of the burned-gas temperature [41]. *EGR* reduces both the oxygen volume concentration and the peak temperature of

216   the burned gases. If the $NO_x$ emissions are plotted as a function of the maximum burned gas temperature of the main

217   shot ($T_{bmax}$ has been calculated by means of a 3 zone combustion model [42]), instead of $[O_2]_{int}$, the pattern observed in

218   Fig. 6 is achieved. However, the best correlation for $NO_x$ is obtained with respect to $[O_2]_{int}$ in Fig. 5.
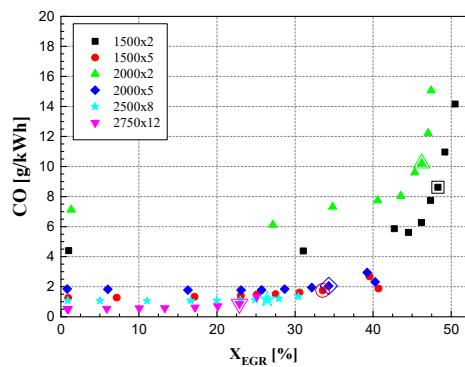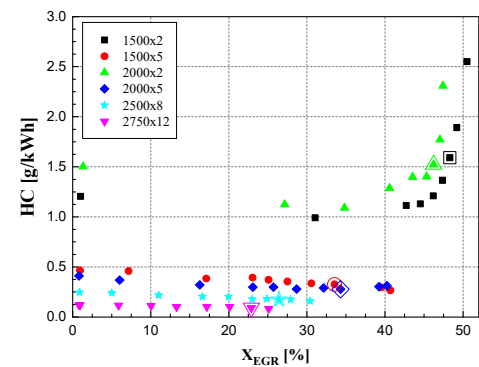


Figure 7. *HC emissions versus $X_{EGR}$.*



Figure 8. *CO emissions versus $X_{EGR}$.*

219 The minimum *EGR* rate that is sufficient to decrease the peak temperature of the burned gas below an acceptable

220 threshold depends on the engine key-point and on the trade-off among different targets (i.e., the limits of different

221 pollutant emissions set by regulations, fuel consumption and combustion noise), as well as on the synergy between

222 combustion strategies and the aftertreatment devices installed in the exhaust pipe. The dilution, chemical and thermal

223 effects of *EGR* simultaneously affect $T_{bmax,main}$ and it is a difficult task to properly split the contribution of each *EGR*

224 effect during normal engine operation conditions because they occur at the same time. The calculations of the thermal

225 properties of air and exhaust gases for the tests considered in the current investigation showed that the specific heat of

226 the *EGR* could be up to 6% higher than the specific heat of the air, whereas the increase in the thermal capacity of the

227 inlet charge was up to 2.5%. This variation is not able to account for the great temperature reduction in the maximum

228 burned gas temperature that can be appreciated by considering both Figs. 4 and 6. Therefore, it can be stated that the

229 dilution and chemical effects are more important than the thermal effect, a result that is in line with the findings in [2].

230 The *CO* and *HC* emissions versus $X_{EGR}$ are plotted in Figs. 7 and 8 and show similar trends, the *CO* emissions being

231 roughly 5 times higher than the corresponding *HC* emissions. In general, *CO* and *HC* emissions reduce as the load

232 increases. In particular, as soon as the combustion temperature exceeds 1400-1500 K, *CO* rapidly oxidizes to $CO_2$ [33,

233 43]. The influence of the *EGR* rate on the *HC* and *CO* emissions is reduced for lower $X_{EGR}$ values than 30%-40%, as can

234 be seen in Figs. 7 and 8. Even the *HC* emissions exhibit a slightly decreasing trend for $X_{EGR}$ up to 35-40% and this trend

235 can be explained considering that the fuel can always find enough air to burn for low $X_{EGR}$ values. As a consequence,

236 the dilution effect of *EGR*, which impacts negatively on *HC* emissions, becomes negligible, while the thermal throttling

237 effect of *EGR* (Fig. 3), which can promote *HC* oxidation, plays a decisive role. *HC* and *CO* emissions increase to a great

238 extent for higher *EGR* mass fractions than 40%, as can be seen in Figs. 7 and 8, due to incomplete combustion. In fact,

239 even though the global λ continues to be lean, the mixture is inhomogeneous and, locally, some fuel cannot find the

240 necessary quantity of air. However, if the turbocharger can provide a sufficiently increased boost pressure, in order to
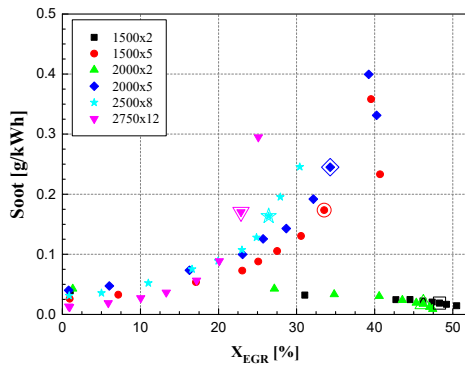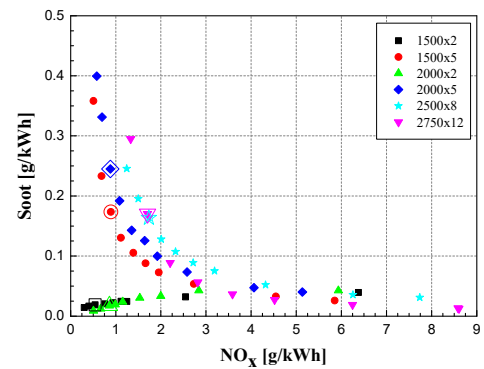


Figure 9. Soot emissions versus $X_{EGR}$.



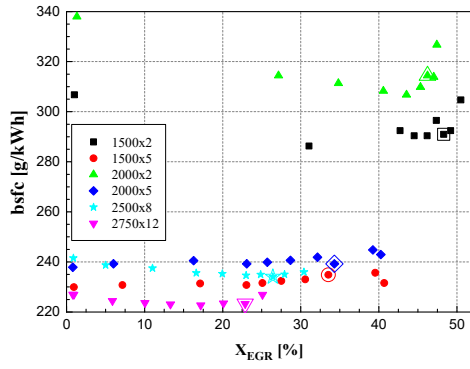Figure 10. $NO_x$-soot curve as $X_{EGR}$ varies.

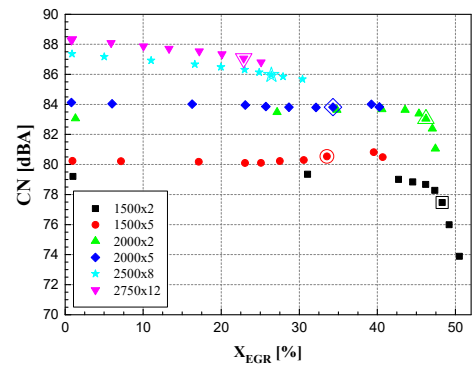Figure 11. Brake specific fuel consumption versus $X_{EGR}$.



Figure 12. Combustion noise versus $X_{EGR}$.

241  maintain adequate local $\phi$ values, the combustion deterioration will practically be negligible. Therefore, almost similar

242  reductions in $NO_x$ as those shown in Fig. 5 would be achieved, but with minor increases in the $CO$ and $HC$ emissions.

243  Soot emissions versus $X_{EGR}$ are plotted in Fig. 9, where different trends, with respect to the $EGR$ rate, can be observed

244  on the basis of the considered load [15]. At the lowest loads ($bmep$ = 2 bar), the soot emissions decrease as $X_{EGR}$

245  increases, but, when the load is increased, it is difficult to employ high $EGR$ rates, due to the deterioration in diffusive

246  combustion, which makes the engine generate more smoke. This sensitivity of soot to $EGR$ at medium and high loads is

247  consistent with the data in [39]. Therefore, a trade-off limit must be set for $X_{EGR}$ at medium and high loads in order to

248  obtain a suitable compromise between $NO_x$ and soot emissions; from this point of view, a high injection pressure or

249  swirl ratio can also be used to suppress soot and allow the $EGR$ limit to be raised [38]. Fig. 10 reports the $NO_x$-soot

250  trade off curves that are obtained for $bmep$ = 5 bar, $bmep$ = 8 bar and $bmep$ = 12 bar by varying $X_{EGR}$. An increase in

251  $X_{EGR}$ has a positive influence on both $NO_x$ and soot emissions at $bmep$ = 2 bar, since the engine works in the $PCCI$

252  regime. However, if the engine is not run under a $PCCI$ type strategy, the presence of the $NO_x$-soot $EGR$ trade-off also

253  persists at low loads [44]. This topic will be dealt with in more detail in section 5, where the in-cylinder analysis is

254  presented.

255  Figure 11 reports $bsfc$ as a function of $X_{EGR}$ for different $bmep$ values. A decrease in $bsfc$ can be found when passing

256  from no $EGR$ to around $X_{EGR} \approx 30\%$ at $bmep$ = 2 bar. This is related to the combustion of the unburned hydrocarbons that

257  enter the combustion chamber with the recirculated exhaust gas [11]. In fact, the exhaust gas contains more $O_2$ at $bmep$

258  = 2 bar than at higher loads. Furthermore, as already mentioned, cooled $EGR$ acts as a pre-heater of the intake mixture.
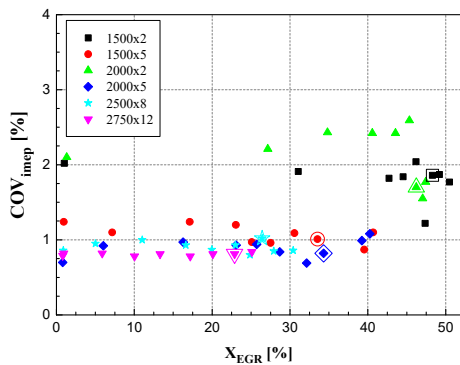

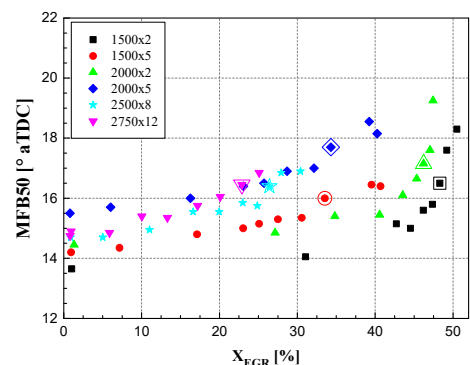
Figure 13. $COV_{imep}$ versus $X_{EGR}$.



Figure 14. Combustion phasing versus $X_{EGR}$.

11

259    When the exhaust gas is recirculated to the cylinder inlet at a low load, the unburned *HC* in the exhaust gas burn

260    because sufficient $O_2$ is available in the combustion chamber and the intake temperatures are relatively high. However,

261    *bsfc* increases with $X_{EGR}$ for heavy *EGR* rates and *bmep* = 2 bar, as there is not enough fresh air to burn all the injected

262    fuel, and this represents a drawback for the use of *EGR* rates beyond $X_{EGR} \approx 40\%$. *bsfc* is less affected by the *EGR* rate at

263    medium and high loads. The influence of *EGR* on the *bsfc* for *bmep* $\geq$ 5 bar does not show a definite trend up to

264    $X_{EGR} \approx 20\%$. A small increase in *bsfc* can be observed for higher *EGR* mass fractions than 20%, mainly due to the

265    reduction in λ and to the longer duration of combustion.

266    Figure 12 plots the combustion noise (*CN*) as a function of $X_{EGR}$. The influence of *EGR* at *bmep* = 2 bar and *bmep* = 5

267    bar, is virtually negligible up to $X_{EGR} \approx 45\%$, whereas an important decrease in *CN* can be found for $X_{EGR} > 45\%$ at

268    *bmep*=2 bar. A continuously decreasing trend can be detected at higher loads, i.e. *bmep* = 8 bar and *bmep* = 12 bar, for

269    $X_{EGR} \leq 30\%$.

270    Combustion stability is not affected to any great extent by the *EGR* rate, since the coefficient of variation of *imep*

271    ($COV_{imep}$) is always lower than 3%, as can be seen in Fig. 13, and no well-defined trend of $COV_{imep}$ with respect to $X_{EGR}$

272    can be observed. Fig. 14 plots the crankshaft angle at which 50% of the mixture has already burned, i.e. *MFB50*, as a

273    function of the *EGR*. The influence on the combustion duration results to be appreciable even for small *EGR* mass

274    fractions and becomes more evident for higher $X_{EGR}$ than 40%. *MFB50* is delayed for all the examined key-points, as

275    $X_{EGR}$ is augmented, since *EGR* slows the chemical reactions.

## 5.   CRANKSHAFT BASED DIAGRAMS FOR THE MAIN IN-CYLINDER QUANTITIES.

277    Figures 15-24 report the unburned gas mass ($M_u$), the in-cylinder pressure ($p_{cyl}$), the *HRR*, the in-cylinder burned zone

278    gas temperature ($T_b$), the $NO_x$ and the soot as functions of the crankshaft angle. The $p_{cyl}$ traces were acquired

279    experimentally using 0.1° CA (crank angle degree) steps and were averaged over 100 consecutive engine cycles; the

280    *HRR* was evaluated by means of a standard 1 zone diagnostic tool on the basis of the $p_{cyl}$ distribution, while the histories

281    of $M_u$, $T_{cyl}$, $NO_x$ and soot were calculated by means of a three-zone diagnostic tool on the basis of the $p_{cyl}$ data. The

282    diagnostic model fitting coefficients were calibrated on the basis of the experimental engine-out emissions [42].
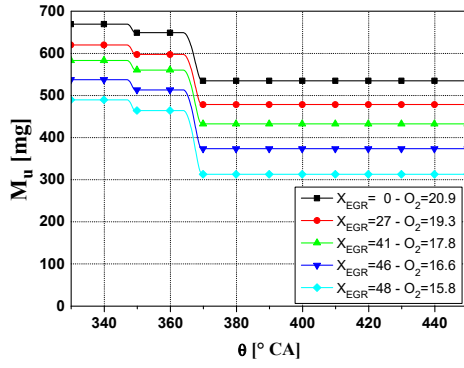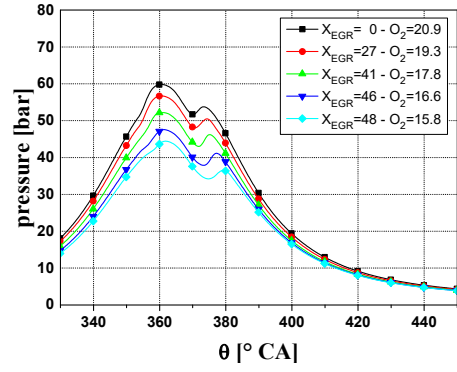
Figure 15. Unburned gas mass as a function of $\theta$ (2000x2).



Figure 16. In-cylinder pressure as a function of $\theta$ (2000x2).

283     The unburned mass $M_u$ accounts for the mixture that has not yet burned at the considered crank angle. Before injection

284     has occurred, $M_u$ is equal to the sum of the inlet fresh air, the *EGR* and the residual gas mass fraction from the previous

285     cycle. As injection takes place, some fuel enters the combustion chamber and mixes with the unburned gases and, as a

286     result, a mixture zone is formed, in which the mass ratio of the air to the fuel is approximately stoichiometric. The

287     unburned mass progressively reduces during the injection and combustion period, as is shown in Fig. 15 for the 2000×2

288     key-point, since part of the initial $M_u$ enters the model mixture zone [42]. The increase in the *EGR* rate makes the value

289     of $M_u$ at $\theta$=330° CA decrease, due to a diminution in the inlet charge density (thermal throttling effect). This reduction

290     in $M_u$ with $X_{EGR}$ determines a reduction in the in-cylinder pressure before combustion, and a more intense reduction
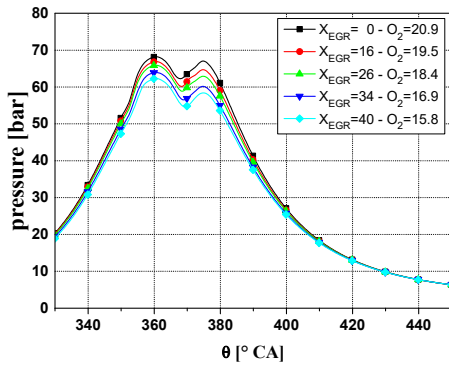


Figure 17. In-cylinder pressure as a function of $\theta$ (2000x5).
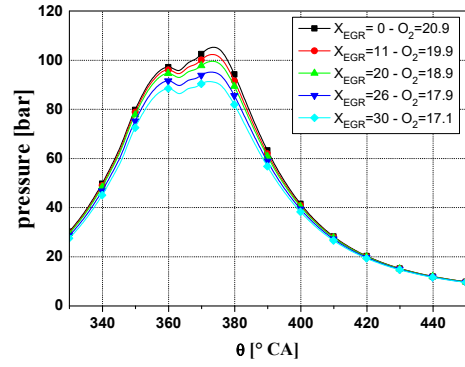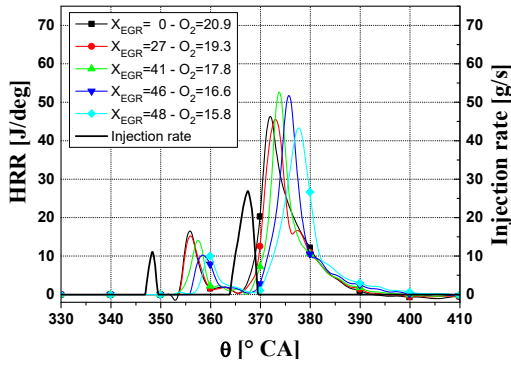


Figure 18. In-cylinder pressure as a function of $\theta$ (2500x8).



Figure 19. Heat release rate as a function of $\theta$ (2000x2).
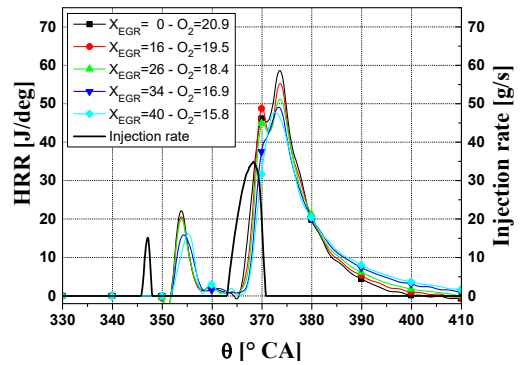


Figure 20. Heat release rate as a function of $\theta$ (2000x5).

13

291 during both the combustion and the early expansion phases (Fig. 16). Less influence of the *EGR* on $p_{cyl}$ is detected as

292 the engine load is increased (Figs. 17 and 18), because combustion is more vigorous and the smaller $X_{EGR}$ values induce

293 lower percentage variations of $M_u$.

294 The *HRR* (thin lines with symbols) and the injection rate (thick solid line) distributions versus the crankshaft angle have

295 been plotted in Fig. 19 for the 2000×2 key-point. Just one injection rate pattern was plotted in order to avoid the

296 overlapping of many curves, but also considering that the variation with *EGR* was minor. The first peak in the *HRR* is

297 related to the pilot injection and is always lower than the second one, which refers to the main combustion. The various

298 changes in the engine inlet charge composition and temperature, due to the *EGR* rate variations, generally alter the fuel

299 mixing with air and the chemical reaction times, that is, the length of the ignition delay. In particular, the ignition delay,

300 which is evaluated as the distance between the start of injection and the corresponding increase in the *HRR* of the pilot

301 injection, tends to lengthen in Fig. 19 when $X_{EGR}$ increases, because the dilution effect prevails over the opposing effect

302 of the increase in the temperature of the inlet charge. However, it is also possible that the two opposite effects balance

303 each other, and in these cases, the ignition delay remains almost unchanged with $X_{EGR}$ [23].

304 The combustion mainly occurs in the premixed phase, as can be seen in Fig 19. In fact, when the combustion of the

305 main injected fuel starts, most of the fuel has already been injected and has had enough time to mix with the in-cylinder

306 charge according to a partial *PCCI* process. Although the increased fuel ignition delay, due to the higher $X_{EGR}$, leads to

307 an increasing amount of fuel that burns in a premixed combustion phase, the reduction in oxygen availability decreases

308 the rate at which the fuel burns in the premixed phase. The prevailing effect depends on the *EGR* rate value and on the

309 considered injection shot (pilot or main).

310 In Fig. 19, it can be observed that, the *HRR* peak always decreases for the pilot injection, whereas the growth in the

311 premixed fraction determines an increased and retarded main combustion *HRR* peak for $X_{EGR}$ values of up to 40-45%,

312 compared to the working condition without *EGR*. When $X_{EGR}$ is increased beyond 45%, the effect of the deceleration of

313 the chemical reaction kinetics prevails over the increased ignition delay and the main combustion *HRR* peak decreases

314 with the *EGR* rate rise. As soon as the load increases, a larger fraction of the mixture burns in the mixing-controlled

315 combustion phase. Furthermore, the ignition delay has been proved to be less sensitive (Fig. 20) or even insensitive to

316 $X_{EGR}$ (Fig. 21); in fact, the unburned gas temperature increases, the combustion reactions become faster and, therefore,

317 the influence of the $[O_2]_{int}$ concentration on the ignition delay becomes marginal. However, the combustion velocity

318 slows down as the *EGR* rate increases, and the intensity of the *HRR* peak that corresponds to the main injection

319 continues to decrease as $X_{EGR}$ rises for medium and high loads.

320 Figure 22 plots the in-cylinder *NO* volume fraction time history (*NO* represents most of the $NO_x$ since $NO_2$ is minor) for

321 the 2000×2 case. The *NO* time distribution was calculated using the extended Zeldovich model [41]. The $NO_{end}/NO_{start}$

14

ratio, where the subscripts *start* and *end* stand for the in-cylinder *NO* volume fraction before the start of combustion

(evaluated at $\theta$=330° CA) and after the end of combustion (evaluated at $\theta$=450° CA), respectively, tends to decrease as

$X_{EGR}$ increases. The absolute value of $NO_{start}$ is proportional to the product of the *EGR* mass and the $NO_{end}$

concentration. When $X_{EGR}$ increases, the *EGR* mass grows, while the fraction of *NO* in this mass, i.e. $NO_{end}$, decreases.

As a result, the absolute value of $NO_{start}$ first increases with $X_{EGR}$ (e.g. from $X_{EGR} = 0$ to $X_{EGR} = 27\%$ in Fig. 22) and then

decreases with it (e.g. from $X_{EGR} = 41\%$ to $X_{EGR} = 48\%$ in Fig. 22).

Figure 23 shows the temperature of the in-cylinder burned gases, which was calculated in the combustion chamber for

different *EGR* mass fractions for the 2000×2 case. The *EGR* reduces the combustion peak temperatures of the burned

gases and is responsible for the massive reduction in the *NO* concentration at the end of combustion (Fig. 22). The

growth in the intake temperature, due to the increase in the *EGR* mass fraction, leads to slightly raised unburned gas

temperatures during the compression phase. This behavior is not in conflict with the decreasing trend of $NO_x$ with $X_{EGR}$,

since the $NO_x$ emissions are closely correlated to the peak temperature of the burned gas zone ($T_{bmax,main}$ around $\theta \approx 360°$

CA in Fig. 23) as well as to the residence time of the burned gases at higher temperatures than 1900-2000 K, but not to

the average gas temperatures in the cylinder.

The soot formation and the soot oxidation phases are outlined in Figs. 24-26. Different engine soot emission trends,

with respect to $X_{EGR}$, can be observed on the basis of the considered load. Soot formation depends on the local

temperature and on $[O_2]_{int}$. The dilution effect of *EGR* has a reduced impact on $[O_2]_{int}$ at low loads (Fig. 24), because of

the relatively high value of λ. On the other hand, an increased *EGR* mass determines a significant reduction in the

burned gas temperature and a consequent reduction in both soot formation and oxidation. The former effect prevails

over the latter, and the soot evaluated at $\theta \approx 450°$ CA results to reduce in Fig. 24 when $X_{EGR}$ is increased. In other words,

most of the fuel is burning under a premixed phase at low loads: fuel, fresh air and *EGR* are mixed thoroughly prior to

combustion, local fuel-rich regions are reduced and combustion temperatures are decreased by *EGR*. On the other hand,
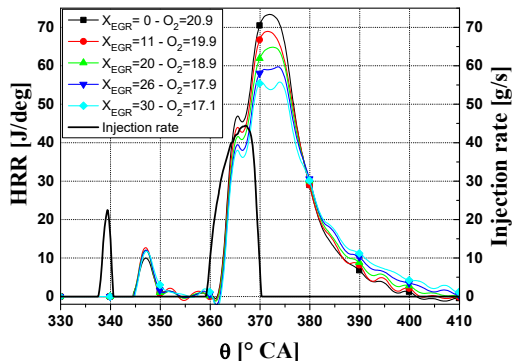


Figure 21. Heat release rate as a function of $\theta$ (2500x8).
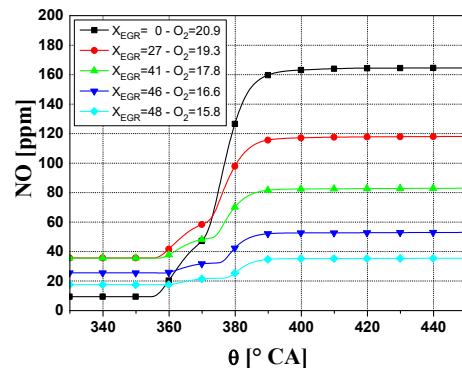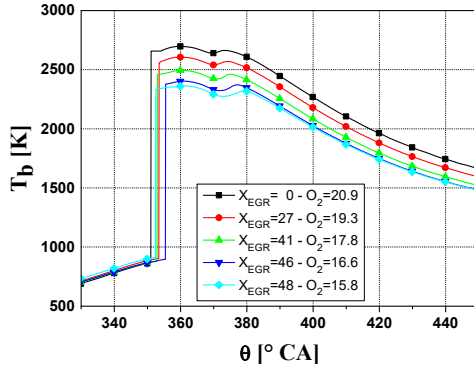


Figure 22. *NO* as a function of $\theta$ (2000x2).
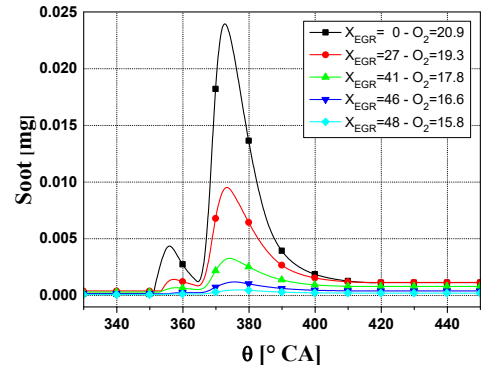
**Figure 23. Burned gas temperature as a function of $\theta$ (2000x2).**
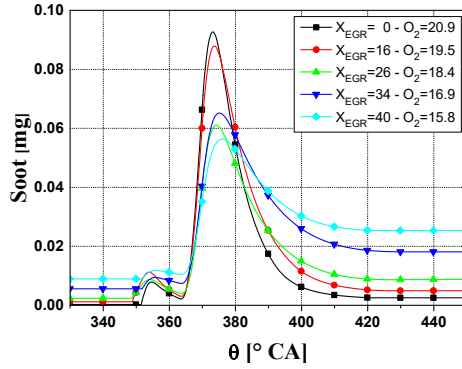


**Figure 24. Soot as a function of $\theta$ (2000x2).**



**Figure 25. Soot as a function of $\theta$ (2000x5).**
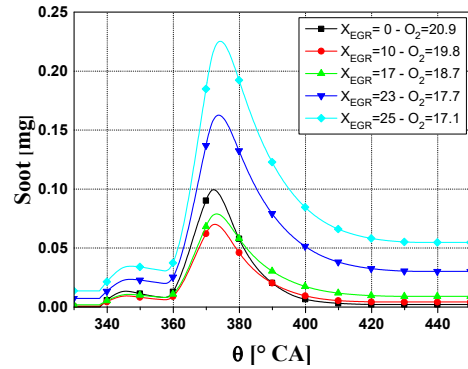


**Figure 26. Soot as a function of $\theta$ (2750x12).**

344    the soot levels observed in Fig. 24 at all the $X_{EGR}$ values are generally not a reason for concern.

345    The soot formation rate for medium loads (*bmep* = 5 in Fig. 25), continues to reduce as the *EGR* rate is increased, but

346    the oxidation rate becomes very low for high *EGR* rates, because of the reduced in-cylinder temperatures. The latter

347    effect becomes the prevailing one in determining the fate of soot, which increases with $X_{EGR}$ at the end of combustion.

348    Finally, at high loads (*bmep* = 12 bar in Fig 26), the augment in $X_{EGR}$ makes λ approach the stoichiometric value, and

349    this effect prevails over the diminution of the burned gas temperatures, and leads to a significantly increased soot

350    formation rate. The soot oxidation rate is negatively affected by *EGR* at high loads, as it is for the low and medium

351    loads. In short, more soot is measured at the engine exhaust when $X_{EGR}$ grows at high loads.

## 6.    CONCLUSIONS.

353    The *EGR* mass fraction has been varied within the 0÷50% range at different steady-state key-points for an automotive

354    Euro 5 low compression ratio diesel engine with an optimized pilot-main double injection strategy, managed with a late

355    *PCCI* type combustion strategy. The selected key-points are representative of the engine application to a vehicle

356    running the *NEDC*. The analysis has been performed considering both the time averaged quantities measured at the test

357    bench and results derived from the application of diagnostic combustion models to the ensemble in-cylinder pressure

358    time history. Attention has been paid to the benefits that high *EGR* rates can have on $NO_x$ reduction and to any possible

359    simultaneous detrimental effects. The largest range of *EGR* rates has been explored without finding an optimal value for

16

360     $X_{EGR}$, which is established as a trade-off between different engine-out emissions and brake specific fuel consumption,

361     but also depends on the synergy between the combustion strategy and the installed aftertreatment devices.

362     The main achievements of the research investigation are synthetically listed hereafter:

363     •     The ignition delay tends to increase at low loads as the EGR increases as a result of the reduction in the oxygen

364     concentration because the EGR dilution effect prevails over the increase in the temperature of the inlet charge (thermal

365     throttling effect). The ignition delay has been proved to be less sensitive or even insensitive to $X_{EGR}$ at medium and high

366     loads because the unburned gas temperature increases, the combustion reactions become faster and the influence of the

367     $[O_2]_{int}$ concentration becomes marginal.

368     •     The *EGR* generally determines an almost linear decrease in $\lambda$ when $X_{EGR}$ increases. However, if

369     high *EGR* rate values, which are typical of *PCCI* type engines, are applied at low loads, a deviation from linearity

370     occurs, since the desired level of boost pressure that is set by the *ECU* cannot be maintained in the intake manifold. In

371     fact, the high mass flow-rate, which is sent back from the exhaust to the intake manifold, determines an insufficient

372     enthalpy flux to the turbine. Furthermore, fresh-air throttling reduces the pressure in the intake manifold.

373     •     The $NO_x$ emission data, referring to the different key-points, are more closely correlated to $[O_2]_{int}$ than to the

374     maximum burned gas temperature. An almost quadratic monotonically increase in $NO_x$ has been found with respect to

375     $[O_2]_{int}$. The combustion timing of the main injection has also been confirmed to have a significant impact on reducing

376     $NO_x$ emissions. The best results, in terms of $NO_x$ reduction, have therefore been achieved in late *PCCI* type strategies,

377     when the combustion timing is retarded and high *EGR* rates are applied.

378     •     The *HC* and *CO* emissions are relevant at low loads for partial *PCCI* engines subjected to heavy *EGR* rates,

379     because fuel over-mixing and wall-quenching occur, due to the very lean mixture and the low temperatures. The

380     influence of *EGR* on these emissions is not so significant, if *EGR* rates of up to 30-40% are applied, as occurs in

381     conventional diesel combustion systems, and, in these conditions, *EGR* can even have a positive effect on *HC*

382     emissions.

383     •     Soot is sensitive to the *EGR* rate and increases exponentially with the *EGR* rate at medium and high conditions.

384     The increase in soot with $X_{EGR}$ is mainly due to the lack of oxygen in the recirculated exhaust gases. It is therefore

385     difficult to employ high *EGR* rates at medium and high loads, due to diffusive combustion deterioration. Therefore, soot

386     and $NO_x$ show a trade-off behavior, with respect to $X_{EGR}$, at medium and high loads. On the other hand, heavy *EGR* rates

387     allow $NO_x$ and soot emissions to be improved simultaneously at low loads, because the low compression ratio engine

388     works in partial *PCCI* mode.

389     •     Brake specific fuel consumption is hardly affected by the *EGR* rate at medium and high loads. The influence of

390     *EGR* on the *bsfc* for $bmep \geq 5$ bar does not show a definite trend up to $X_{EGR} \approx 20\%$. A small increase in *bsfc* can be

observed for higher *EGR* mass fractions than 20%, mainly due to the reduction in $\lambda$ and to the longer duration of combustion. Instead, a decrease in *bsfc* can be found when passing from no *EGR* to around $X_{EGR}\approx30\%$ at low loads. This is related to the combustion of the unburned hydrocarbons that enter the combustion chamber with the cooled *EGR*, which involves more $O_2$ at low loads than at higher loads and acts as a pre-heater of the intake mixture. However, *bsfc* increases with $X_{EGR}$ for heavy *EGR* rates at low loads, due to a lack of fresh air, which is necessary to burn all the injected fuel, and this represents a drawback for the use of high *EGR* rates in *PCCI* strategies.

• The stability of the combustion is not affected significantly by the *EGR* rate: the coefficient of variation of the *imep* is always lower than 3% for all the considered *EGR* mass fractions. The increase in the *EGR* rate generally makes the combustion noise decrease, but the effectiveness of this measure depends on the engine load and on the *EGR* rate. An important reduction in *CN* occurs under heavy *EGR* rates for the *PCCI* working mode.

# 7.   NOMENCLATURE

*bmep*          brake mean effective pressure

*bsfc*          brake specific fuel consumption

*CA*            crank angle

*CN*            combustion noise

$COV_{imep}$    coefficient of variation for the specific torque

$[CO_2]_{amb}$  volume concentration of $CO_2$ in the external environment

$[CO_2]_{exh}$  volume concentration of $CO_2$ in the engine exhaust

$[CO_2]_{int}$  volume concentration of $CO_2$ in the intake manifold

*ECU*           electronic control unit

*EGR*           exhaust gas recirculation

*HC*            unburned hydrocarbons

*HCCI*          homogeneous charge compression ignition

*HRR*           heat release rate

*imep*          indicated mean effective pressure

*LTC*           low-temperature combustion

$\dot{m}_a$     fresh air mass flow-rate

$\dot{m}_{EGR}$ exhaust gas mass flow-rate

$M_u$           unburned gas mass

| 420 | *MFB50* | angle at which 50% of the combustion mixture has burned |
| 421 | *n* | engine speed |
| 422 | $NO_{start}$ | *NO* emissions before the start of combustion |
| 423 | $NO_{end}$ | *NO* emissions after the end of combustion |
| 424 | $NO_x$ | nitrogen oxides |
| 425 | $[O_2]_{int}$ | oxygen volume concentration in the intake manifold |
| 426 | $p_{int}$ | pressure in the intake manifold (boost pressure) |
| 427 | $p_{cyl}$ | in-cylinder pressure |
| 428 | *PCCI* | partial premixed charge compression ignition |
| 429 | *PM* | particulate matter |
| 430 | $q_{pil}$ | volume of fuel injected in the pilot injection |
| 431 | $SOI_{Main}$ | electrical start of the main injection |
| 432 | $SOI_{Pil}$ | electrical start of the pilot injection |
| 433 | $T_b$ | in-cylinder burned gas temperature |
| 434 | $T_{bmax,main}$ | maximum in-cylinder burned gas temperature |
| 435 | *TDC* | top dead center |
| 436 | $X_{EGR}$ | mass fraction of exhaust gas recirculation |
| 437 | $\phi$ | equivalence ratio |
| 438 | $\lambda$ | relative air-fuel ratio |
| 439 | $\theta$ | crankshaft angle |

440 **8.  REFERENCES.**

441  [1]  Zheng M, Reader GT, Hawley JG. Diesel engine exhaust gas recirculation—a review on advanced and novel
442      concepts. *Energy Conversion and Management*, 2004, vol. 45, pp. 883–900.

443  [2]  Ladommatos N, Abdelhalim SM, Zhao H, Hu Z. Effects of EGR on Heat release in Diesel Combustion. SAE
444      Paper No. 980184.

445  [3]  Pickett LM and Siebers DL. Non-Sooting Low Flame Temperature Mixing-Controlled DI Diesel Combustion.
446      SAE Paper No. 2004-01-1399

447  [4]  Lapuerta M, Hernandez JJ, Gimenez F. Evaluation of exhaust gas recirculation as a technique for reducing diesel
448      engine $NO_x$ emissions. *Proc Instn Mech Engrs part D J Autom Engns*, 2000, vol 214, pp. 85-93.

449  [5]  Heywood JB. Internal Combustion Engine Fundamentals. New York, McGraw-Hill International Editions, 1988.

450     [6]    Zelenka P, Aufinger H, Reczek W, Catellieri W. Cooled EGR—a key technology for future efficient HD Diesels.

451            SAE Paper No. 980190.

452     [7]    Kreso AM, Johnson JH, Gratz LD, Bagley ST, Leddy DG. A study of the effects of exhaust gas recirculation on

453            heavy-duty Diesel engine emissions. SAE Paper No. 981422.

454     [8]    Maiboom A, Tauzia X, Helet J. Experimental study of various effects of exhaust gas recirculation (EGR) on

455            combustion and emissions of an automotive direct injection diesel engine, *Energy*, 2008, vol. 33, pp. 22-34..

456     [9]    Abd-Alla GH., Using exhaust gas recirculation in internal combustion engines: a review, *Energy Conversion and*

457            *Management*, 2002, vol. 43, pp. 1027–1042.

458     [10]   Ladommatos N, Abdelhalim SM, Zhao H, Hu Z. The effects of carbon dioxide in exhaust gas recirculation on

459            diesel engine emissions. *Proc Instn Mech Engrs part D J Autom Engns*, 1998, vol. 212, pp. 25-42.

460     [11]   Agarwal D., Singh SK., Agarwal AK. Effect of Exhaust Gas Recirculation (EGR) on performance, emissions,

461            deposits and durability of a constant speed compression ignition engine. *Applied Energy*, 2011, vol. 88, pp. 2900–

462            2907.

463     [12]   Hountalas DT, Mavropoulos GC, Binder KB. Effect of exhaust gas recirculation (EGR) temperature for various

464            EGR rates on heavy duty DI diesel engine performance and emissions. *Energy*, 2008, vol. 33, pp. 272–283.

465     [13]   Park, Y., and Bae, C., 2014. Experimental study on the effects of high/low pressure EGR proportion in a passenger

466            car diesel engine. *Applied Energy*, 2014, vol.133, pp. 308-316.

467     [14]   Reader GT, Galinsky G, Potter I, Gustafson RW. Combustion noise levels and frequency spectra in an IDI Diesel

468            engine using modified intake mixtures. *Emerging Energy Technol Trans ASME*, 1995, vol.66, pp. 53–58.

469     [15]   Kouremenos D. A., Hountalas D. T., Binder K. B., The Effect of EGR on the Performance and Pollutant

470            Emissions of Heavy Duty Diesel Engines using Constant and Variable AFR, SAE Paper No. 2001-01-0198.

471     [16]   McKinley TL. Modeling Sulfuric Acid Condensation in Diesel Engine EGR Coolers. SAE Paper No. 970636.

472     [17]   Lim J, Kang B, Park J, Yeom Y, Chung S, Ha J. A Study on Exhaust Characteristics in HSDI Diesel Engine Using

473            EGR Cooler. Proceedings of the KSAE 2004 Fall Conference, pp. 306–312.

474     [18]   Schubiger R, Bertola A, Boulouchos K. Influence of EGR on Combustion and Exhaust Emissions of Heavy Duty

475            DI-Diesel Engines equipped with Common-Rail Injection Systems. SAE Paper No. 2001-01-3497.

476     [19]   Dennis AJ., Garrner CP., Taylor DHC. The Effect of EGR on Diesel Engine Wear. SAE Paper No. 1999-01-0839.

477     [20]   Ishiki K, Oshida S, Takiguchi M. A study of abnormal wear in power cylinder of diesel engine with EGR-wear

478            mechanism of soot contaminated in lubricating oil. SAE Paper No. 2000-01-0925.

479     [21]   Agarwal AK, Singh SK, Sinha S, Shukla MK. Effect of EGR on the exhaust gas temperature and exhaust opacity

480            in compression ignition engines. *Sadhana* Vol. 29, Part 3, June 2004, pp. 275–284.

481 [22] Ladommatos N, Abdelhalim SM, Zhao H, Hu Z. The Dilution, Chemical, and Thermal Effects of Exhaust Gas
482      Recirculation on Diesel Engine Emissions - Part 4: Effects of Carbon Dioxide and Water Vapour. SAE Paper No.
483      971660.

484 [23] Jacobs T, Assanis D, Filipi Z. The Impact of Exhaust Gas Recirculation on Performance and Emissions of a
485      Heavy-Duty Diesel Engine. SAE Paper No. 2003-01-1068.

486 [24] Wilson RP, Muir EB, Pellicciotti FA. Emissions study of a single-cylinder diesel engine, SAE paper No. 740123.

487 [25] Zhu Y, Ricart-Ugaz L, Wu S, Cigler J, El-Beshbeeshy M, Bulicz T, Yan J. Combustion Development of the New
488      International 6.0L V8 Diesel Engine. SAE Paper No 2004-01-1404.

489 [26] Nitu B, Singh I, Zhong L, Badreshany K, Henein NA, Bryzik W. Effect of EGR on autoignition, combustion,
490      regulated emissions, and ldehydes in DI diesel engines. SAE paper no. 2002-01-1153.

491 [27] Uchida N, Daisho Y, Saito T, Sugano H. Combined Effects of EGR and Supercharging on Diesel Combustion and
492      Emissions. SAE Paper No. 930601.

493 [28] Park J, Song S, Lee KS. Numerical investigation of a dual-loop EGR split strategy using a split index and multi-
494      objective Pareto optimization. *Applied Energy*, 2015, vol. 142, pp. 21-32.

495 [29] Verschaeren, R., Schaepdryver, W., Serruys, T., Bastiaen, M., Vervaeke, L., Verhelst, S. Experimental study of
496      $NO_x$ reduction on a medium speed heavy duty diesel engine by the application of EGR (exhaust gas recirculation)
497      and Miller timing, *Energy*, 2014, vol. 76, pp. 614-621.

498 [30] Yao M, Zheng Z, Liu H. Progress and recent trends in homogeneous charge compression ignition (*HCCI*) engines.
499      *Progress in Energy and Combustion Science*, 2009, vol. 35, pp. 398–437.

500 [31] Saxena S, Bedoya ID. Fundamental phenomena affecting low temperature combustion and HCCI engines, high
501      load limits and strategies for extending these limits. *Progress in Energy and Combustion Science*, 2013, vol. 39,
502      pp. 457-488, http://dx.doi.org/10.1016/j.pecs.2013.05.002.

503 [32] Fang Q, Fang J, Zhuang J, Huang., A. Influences of pilot injection and exhaust gas recirculation on combustion
504      and emissions in a HCCI-DI combustion engine. *Applied Thermal Engineering*, 2012, vol. 48, pp. 97-104.

505 [33] Han D, Ickes AM, Bohac SV, Huang A, Assanis DN. HC and CO emissions of premixed low-temperature
506      combustion fueled by blends of diesel and gasoline. *Fuel*, 2012, 99, pp. 13–19.

507 [34] Sethi VP, Salariya KS. Exhaust Analysis and Performance of a Single Cylinder Diesel Engine Run on Dual Fuels.
508      *IE(I) Journal-MC*, vol 85, April 2004.

509 [35] L. Cornolti, A. Onorati, T. Cerri, G. Montenegro, F. Piscaglia. 1D simulation of a turbocharged Diesel engine with
510      comparison of short and long EGR route solutions. *Applied Energy*, vol. 111, 2013, pp. 1-15.

[36] d'Ambrosio S, Ferrari A, Spessa E. Analysis of the Exhaust Gas Recirculation System Performance in Modern Diesel Engines. *Journal of Engineering for Gas Turbines and Power*, 2013, Vol. 135, pp. 0816011-08160113.

[37] R. Manimaran, R. Thundil Karuppa Raj, CFD Analysis of Combustion and Pollutant Formation Phenomena in a Direct Injection Diesel Engine at Different EGR Conditions, *Procedia Engineering*, 2013, vol. 64, pp. 497-506.

[38] Lee Y., Huh, K. Y. Analysis of different modes of low temperature combustion by ultra-high EGR and modulated kinetics in a heavy duty diesel engine. *Applied Thermal Engineering*, 2014, vol. 70 (1), pp. 776-787.

[39] Zheng, Z., Yue, L., Liu, H., Zhu, Y., Zhong, X., Yao, M. Effect of two-stage injection on combustion and emissions under high EGR rate on a diesel engine by fueling blends of diesel/gasoline, diesel/n-butanol, diesel/gasoline/n-butanol and pure diesel. *Energy Conversion and Management*, 2015, vol. 90, pp. 1-11

[40] d'Ambrosio S, Finesso R, Spessa E. Calculation Of Mass Emissions, Oxygen Mass Fraction And Thermal Capacity Of The Inducted Charge In SI And Diesel Engines From Exhaust And Intake Gas Analysis. *Fuel*, 2011, n. 90, issue 1, pp. 152-166.

[41] d'Ambrosio S., Finesso R., Fu L., Mittica A. and Spessa E., A control-oriented real-time semi-empirical model for the prediction of NOx emissions in diesel engines. *Applied Energy*, 2014, vol. 130, pp. 265–279.

[42] Finesso R, Spessa E. A real time zero-dimensional diagnostic model for the calculation of in-cylinder temperatures, HRR and nitrogen oxides in diesel engines. *Energy Convers Manage*, 2014, vol.79, pp. 498–510.

[43] Liu H, Li S., Zheng Z, Xu J, Yao M. Effects of n-butanol, 2-butanol, and methyl octynoate addition to diesel fuel on combustion and emissions over a wide range of exhaust gas recirculation (EGR) rates. *Applied Energy*, 2013, vol. 112, pp. 246–256

[44] Zamboni, G., Capobianco, M. Influence of high and low pressure EGR and VGT control on in-cylinder pressure diagrams and rate of heat release in an automotive turbocharged diesel engine. *Applied Thermal Engineering*, 2013, vol. 51 (1–2), pp. 586-596.